A Research on PPE Lens Antennas with Matching Layers for Multi-Beam Generation

Nguyen Thi Dieu Linh [1], Phan Van Hung [2], Nguyen Quoc Dinh [3], and T. V. Luyen [4,*]

[1] Department of Science and Technology, Hanoi University of Industry, Hanoi, Vietnam
[2] Faculty of Telecommunications, Telecommunications University, Khanhhoa, Vietnam
[3] Advanced Wireless Communications Group, Le Quy Don Technical University, Hanoi, Vietnam
[4] Faculty of Electronic Engineering, Hanoi University of Industry, Hanoi, Vietnam
Email: linhntd@haui.edu.vn (N.T.D.L.); phanvanhung@tcu.edu.vn (P.V.H.); dinhnq@lqdtu.edu.vn (N.Q.D.); luyentv@haui.edu.vn (T.V.L.)
*Corresponding author

***Abstract*—Lens antennas are considered promising antenna structures for next-generation communication systems due to their high radiation characteristics, low Side-Lobe Level (SLL), and ability to generate multiple beams. In this paper, the authors propose using the modified Polyphenylene Ether (PPE) lens antenna with Matching Layers (MLs) applied to both the inner and outer surfaces of four lens structures: hyperbolic, plano-convex, Abbe sine condition, and straight-line condition. Through the analysis and evaluation of the simulation results, it can be observed that the proposed lens antenna structures with matching layers exhibit high gain values, superior to those of lens antenna structures without matching layers. The maximum gain of the lens antenna with the Abbe sine condition is 27.83 dBi, while the maximum gain values of the plano-convex, hyperbolic, and straight-line lens antennas are 27.82 dBi, 27.73 dBi, and 27.74 dBi, respectively. Additionally, in this paper, the authors set up multiple feed horns along a defined trajectory. The results show that the lens antenna with matching layers is capable of generating multiple beams, with a maximum gain of 22.77 dBi at an incident angle of 45°.**

***Keywords*—lens antenna, matching layer, multi-beam**

I. Introduction

Wireless communication has advanced rapidly over the past few decades. The progression from 1G to 4G has significantly transformed our perception of the world and interactions with others. However, as wireless connections proliferate and users demand higher data rates and lower latency, researchers and manufacturers have developed a new communication system called 5G [1–3].

One of the key challenges in high-frequency communication systems lies in the design and development of transmitters and receivers, where antennas play a vital role. Unlike traditional antennas used in 4G and earlier generations, 5G antennas must exhibit high directionality to minimize space loss, support the generation of multiple beams, and enable real-time beam steering and beamforming [4].

The fifth-generation mobile system is being developed worldwide [1−3]. Key features of 5G in radio wave technology include millimeter wave frequencies, small-sized cells, and Multiple Input Multiple Output (MIMO) systems [5, 6]. This new technology enables 5G antennas to achieve low latency, path loss, multi-beam capabilities, beam scanning, broadband, and a stable radiation pattern. In massive MIMO, the base station antenna assigns a dedicated access line and corresponding radio beam to each user [7, 8].

Therefore, the base station antenna must have a multi-beam radiation pattern. Utilizing millimeter wave technology reduces the size of the base station antenna to approximately 30 cm, leading to the proposal of various antenna types, including reflector antennas, phased arrays, and dielectric lens antennas. For reflector antennas, bifocal dual reflectors and reflect arrays are suggested for multi-beam applications [9, 10]. Phased array antennas are combined with meta surface lenses to enhance angular scanning range, broadband capabilities, and multi-beam functionality [11−18].

Consequently, a lens antenna with a specialized structure, free from feed element blockages, shows great promise for 5G mobile communication systems. It facilitates the generation of multiple beams and enables beam steering with high directivity [19–27].

In dielectric lens antenna applications, selecting the right relative permittivity for the lens material is crucial. This factor significantly affects the antenna's radiation characteristics. Dense materials like Mica, modified PPE, and Silicon improve energy transmission through the lens. They also enhance the antenna's front-to-back radiation ratio. However, using dense dielectric materials can cause reflections at the interface between the air and the dielectric layer. These reflections may negatively impact input impedance [28−30]. As a result, they can reduce gain, distort the beam, and increase side-lobe levels, all of which degrade antenna performance. ML techniques are applied to mitigate these issues and improve the efficiency and performance of lens antennas in communication systems [31, 32].

This study proposes a PPE dielectric lens antenna structure with two Matching Layers (MLs). These layers

Manuscript received January 27, 2025; revised February 28, 2025, accepted March 20, 2025; published July 16, 2025.

are applied to both the inner and outer surfaces of the lens. The multi-beam capability of the lens antenna with this proposed structure is also evaluated.

The paper is organized into five sections. Section II discusses lens reflection, while Section III presents models of lens antenna structures with matching layers and their multi-beam capability. Section IV provides the simulation results and their evaluation, and Section V presents the conclusion of the study.

II. Reflection of a Lens

When electromagnetic waves interact with an object, their energy is divided into three fundamental forms: reflection, transmission, and absorption. The proportions of these energy types are governed by the dielectric properties of the material. The complex permittivity constant is described by the following equation:

$$\varepsilon = \varepsilon' - j\varepsilon'' \tag{1}$$

The real part ε' of the complex permittivity constant is called the dielectric constant, representing the material's ability to store electrical energy. The imaginary part ε'' is known as the loss factor, indicating the energy loss within the material due to the electric field. Reflection loss refers to the portion of energy reflected back to the source or in an undesired direction. In lens antennas, reflection occurs at the interface between the lens material and air. Reflection loss is caused by the change or mismatch in dielectric properties between the lens material and air. Reflection loss depends on the angle of incidence of the wave at the lens-air interface. Increasing the angle of incidence raises the reflection coefficient, and when the rays reach the critical angle, total reflection occurs.

Dielectric lens antennas are made from materials with high electron density, such as Mica and modified polyphenylene ether (modified-PPE). These materials enhance energy transmission efficiency through the lens and improve the antenna's front-to-back radiation ratio. However, using high electron density dielectric materials can cause reflections on the lens surface. These reflections occur between the air layer and the dielectric layer of the lens. As a result, they can significantly affect the input impedance of the feed [28, 29]. They also impact the lens antenna's performance by reducing gain, distorting the beam, and increasing side-lobe levels. These undesirable effects may limit the effectiveness of matching layers [30, 31]. The matching layer is a dielectric layer applied to the surface of the lens. It acts as an intermediary between the air medium and the dielectric material of the lens. Fig. 1 shows the position of the matching layer applied to the dielectric layer of the lens. Accordingly, region 1 represents the air, region 2 is the matching layer, region 3 is the dielectric material, and region 4 is the ML. Here, r_{ij} is the energy reflection coefficient at the interface between regions i and j; r_{12} and r_{23} are the reflection coefficients at the interfaces between regions 1 and 2 and regions 2 and 3, respectively. The energy reflection coefficient is determined by the equations [33]:

$$r_{ij} = \left| \frac{\sqrt{\varepsilon_i} - \sqrt{\varepsilon_j}}{\sqrt{\varepsilon_i} + \sqrt{\varepsilon_j}} \right| \tag{2}$$

$$R = \frac{(r_{12} + r_{23})^2 - 4r_{12}r_{23}\sin^2 \alpha_k d}{(1 + r_{12}r_{23})^2 - 4r_{12}r_{23}\sin^2 \alpha_k d} \tag{3}$$

where, $\alpha_k = 2\pi/\lambda_{ML}$, with λ_{ML} being the wavelength in the ML medium. If ε_{ML} lies between ε_1 and ε_r, then $r_{12}r_{23}$ is positive, causing R to change as a function of the ML thickness (d). Therefore, R reaches its minimum value when $d = \lambda_{ML}/4$ and becomes zero when $r_{12} = r_{23}$, which point ε_{ML} the geometric mean of ε_1 and ε_r or $\varepsilon_{ML} = \sqrt{\varepsilon_1 \varepsilon_r}$.

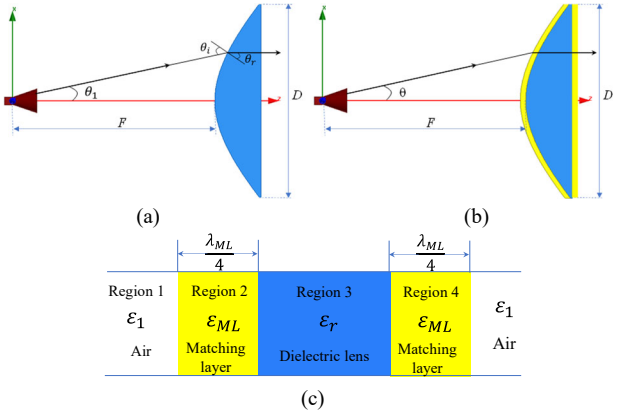

Fig. 1. The structure of the lens antenna with and without the ML, (a). Dielectric lens without ML, (b). Dielectric lens with MLs, (c) A slide section of lens with MLs.

The thickness of the ML is determined by the following Eq. (4):

$$d = \frac{\lambda_{ML}}{4} = \frac{\lambda}{4n_{ML}} \tag{4}$$

where λ is the wavelength in free space, and n_{ML} is the refractive index of the ML. Under these conditions, all energy is transmitted from medium 1 into medium 2, with no energy reflected at the surface.

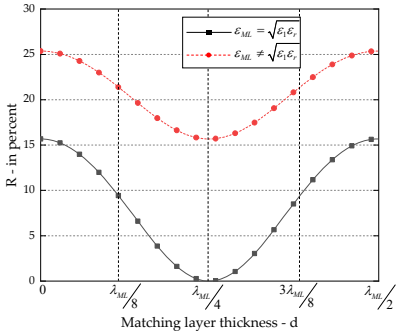

Fig. 2. Power reflection coefficients.

Fig. 2 illustrates the effect of the matching layer's thickness and dielectric constant on the energy reflection coefficient of the lens antenna. The results show that the reflection coefficient reaches its minimum when the dielectric constant of the Matching Layer (ML) is the

geometric mean of the two media: air and the lens material. This occurs when the ML thickness is a quarter-wavelength in the ML medium. The reflection coefficient becomes zero when the lens surface is flat, as represented by the solid black line with square markers. However, when the dielectric constant of the ML differs from the geometric mean of ε_1 and ε_r ($\varepsilon_{ML} \neq \sqrt{\varepsilon_1 \varepsilon_r}$), the energy reflection coefficient reaches a minimum when $d = \lambda_{ML}/4$, but it cannot completely eliminate the reflected energy.

III. Lens Antenna Structure

The lens antenna structure models used in this paper are of the external feed lens antenna type, as shown in Fig. 3. That is, the feed does not directly contact the lens and is placed at the focal point, at a distance *F* from the lens. The lens has a circular structure that rotates around the radiation axis *Oz* (optical axis) and has a diameter *D*. The ratio between the diameter *D* and the distance *F* of the lens is set to one (*F/D* = 1). The thickness of the lens (*T*) is the largest dimension of the lens along the antenna's radiation direction, measured from the inner to the outer radiation surface of the lens.

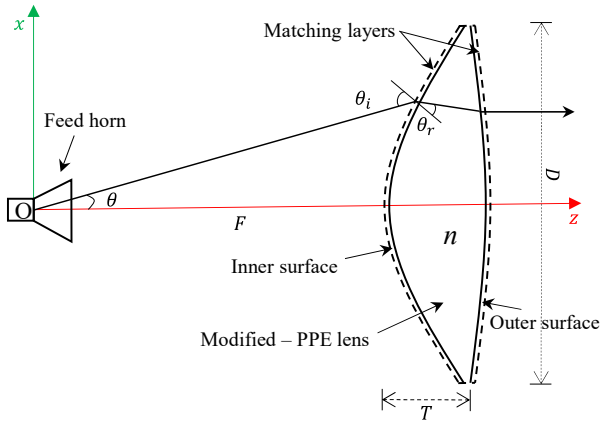

Fig. 3. Lens antenna structure with matching layers.

The refractive index of the lens is given by the Eq. (5):

$$n = \sqrt{\varepsilon_r \mu_r} \tag{5}$$

where ε_r is the relative permittivity, and μ_r is the relative permeability of the lens material.

This study proposes using quarter-wavelength matching layers on both the front and rear surfaces of four types of lenses. These lenses include Hyperbolic, Plano-Convex, Abbe sine condition, and Straight-line condition. Additionally, an off-axis radiation source is positioned along a specified trajectory to generate multiple beams for the proposed lens antenna structures. Dielectric materials used for lenses are typically selected based on their relative permittivity (ε_r), which generally ranges from 1.2 to 12. Low-permittivity materials, such as Teflon (ε_r = 2.2) is commonly material, have a low dielectric electron density but exhibit limited energy transmission from the front to the back of the lens. In contrast, high-permittivity materials, such as Silicon (ε_r = 11.9) and Alumina (ε_r = 9.2), provide high energy transmission capabilities but are significantly affected by surface reflections. Therefore, in this study, modified polyphenylene ether (ε_r = 5.34, μ_r = 1, *tanδ* = 0.0081) is chosen as the lens material due to its moderate dielectric electron density, good energy transmission properties.

A. Feed for Lens Antennas

In this study, the horn antenna serves as a wide−angle radiation source for the lens antenna. The graph showing the reflection coefficient S11 of the horn antenna is presented in Fig. 4. The horn antenna is designed to operate in the N257 band, which ranges from 26.50 GHz to 29.50 GHz, with a center frequency of 28 GHz, a frequency range designated for 5G mobile communication. The horn antenna has a maximum gain of 15.15 dBi and is capable of directing over 90% of the radiated energy into the lens when its phase center is positioned at the lens's focal point.

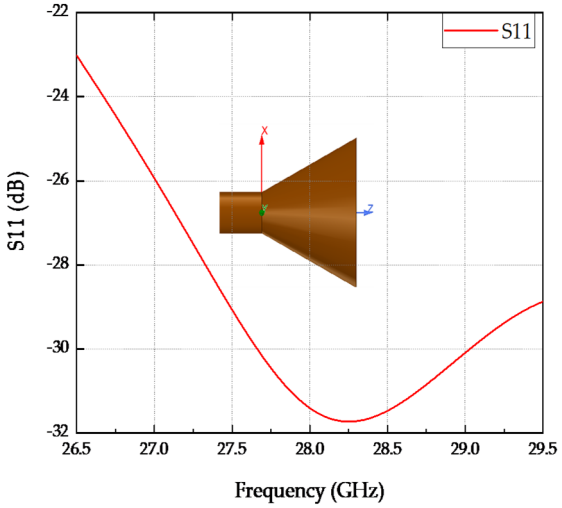

Fig. 4. Reflection coefficient of the horn antenna in the N257 band.

B. Lens Structures

1) Hyperbolic lens structure

The hyperbolic lens features a refractive surface with a distinct structure. Its inner surface is curved, while the outer surface remains flat. The inner curved surface follows a hyperbolic shape (S_I) and is defined by the following Eq. (6) [34, 35].

$$r = \frac{(n-1)F}{n\cos\theta - 1} \tag{6}$$

In this equation, *r* is the distance from the focal point to the curved surface of the lens. The focal point of the lens is placed at the phase center of the horn antenna. *F* is the distance from the focal point to the apex of the lens (the apex is the point where the inner curve of the lens intersects the radiation axis *Oz*). θ is the angle formed by the ray from the focal point to the curved surface of the lens and the radiation axis *Oz*. *x* is the distance from any point on the open surface to the Oz axis, and is given by the equation $x = r\sin(\theta)$. From Eq. (6), *x* is expressed in the following forms:

$$x = \frac{(n-1)F\sin(\theta)}{n\cos\theta - 1} \tag{7}$$

$$\frac{dx}{d\theta} = \frac{(n-1)F(n-\cos\theta)}{(n\cos\theta - 1)^2} \tag{8}$$

By applying Eqs. (6−8), the inner curved surface and the structure of the hyperbolic lens can be determined, as shown in Fig. 5.

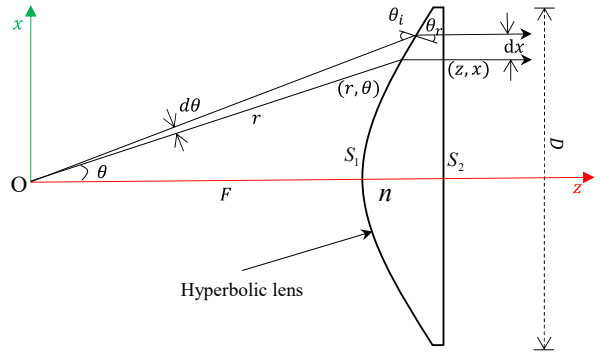

Fig. 5. Hyperbolic lens structure.

2) Plano-convex lens structure

Fig. 6 shows the structure of the dielectric lens with a plano-convex shape. The inner surface (S_1) is flat, while the outer surface (S_2) is convex. The outer surface of the lens is defined by the coordinates (F, x_1), where $z_1 = F$ (the focal length of the lens). The convex surface S_2 is described by the coordinates (z_2, x_2), as detailed in [36].

$$z_2 = \frac{\left[(n-1)T - \sqrt{F^2 + x_1^2}\right]\sqrt{(n^2-1)x_1^2 + n^2F^2} + n^2\sqrt{F^2 + x_1^2}}{n^2\sqrt{F^2 + x_1^2} - \sqrt{(n^2-1)x_1^2 + n^2F^2}} \tag{9}$$

$$x_2 = x_1\left[1 + \frac{z_2 - F}{\sqrt{(n^2-1)x_1^2 + n^2F^2}}\right] \tag{10}$$

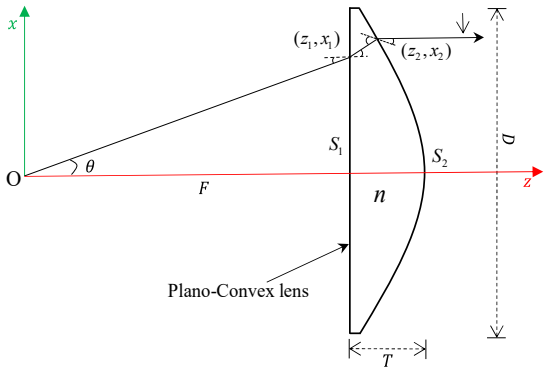

Fig. 6. Plano-Convex lens structure.

3) Abbe sine condition lens structure

The lens, designed according to the Abbe sine condition, is a bi-convex lens with a circular structure around the Oz axis, as shown in Fig. 7. The two surfaces of the lens are defined using the ray tracing method. This method involves calculating factors such as the angle of refraction and the path of the wave ray from the radiation source to the lens aperture [35, 37, 38]. The inner curved surface of the lens (S_1) is described by Eq. (11).

$$\frac{dr}{d\theta} = \frac{rn\sin(\theta - \theta')}{n\cos(\theta - \theta') - 1} \tag{11}$$

In this equation, θ' is the angle formed by the refracted ray after the curved surface S_1 and the radiation axis.

The structure of the outer surface (S_2) of the lens is determined based on the Eq. (12):

$$\frac{dz}{d\theta} = \frac{n\sin\theta'}{1 - n\cos\theta'}\frac{dx}{d\theta} \tag{12}$$

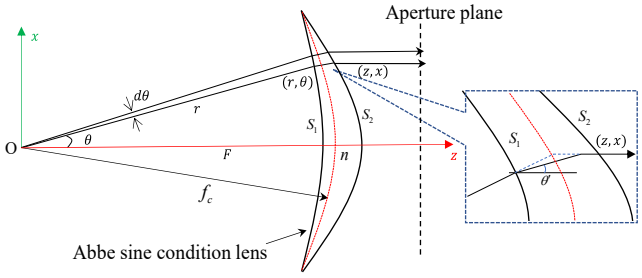

Fig .7. Abbe sine condition lens structure.

To satisfy the Abbe sine condition, the wave rays from the radiation source and the wave rays extending from the lens aperture intersect at a point on a circular arc with a radius of f_c, represented by the red dashed curve in Fig. 7. The circular arc in the xOz plane is defined by the following Eq. (13):

$$\frac{dx}{d\theta} = f_c\cos\theta \tag{13}$$

By simultaneously solving the three differential Eqs. (11−13), we can determine the structure of the inner and outer surfaces of the lens that satisfies the Abbe sine condition.

4) Straight-line condition lens structure

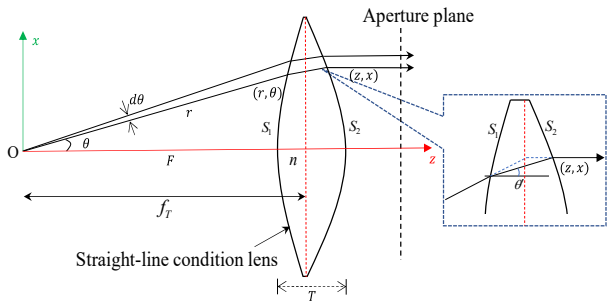

Fig. 8. Straight-line condition lens structure.

Similar to the Abbe sine condition lens, the Straight-line condition lens is a bi-convex lens with a circular structure around the Oz axis. Its two curved surfaces are defined by Eqs. (11−12). To satisfy the straight-line condition, the lens structure must meet a specific requirement. The rays from the radiation source and those extending from the lens aperture must intersect at a point on a straight-line. This line is located at a distance of f_T from the focal point,

as shown by the red dashed line in Fig. 8. The value of f_T is determined by the following Eq. (14).

$$\frac{dx}{d\theta} = \frac{f_T}{\cos^2\theta} \tag{14}$$

IV. Result and Discussion

The study utilizes the advanced electromagnetic field calculation software Ansys HFSS to model, simulate, and compute the lens antenna structure with the proposed designs. Additionally, the authors apply the Finite Element-Based Spatial Analysis Technique (FEBI) in combination with the adaptive mesh refinement algorithm and the Multi-Level Fast Multipole Method (MLFMM) to improve computation time and result accuracy. The structural parameters of the lens and the simulation methods used for the calculations are presented in Table I.

TABLE I. Simulation Parameters and Method

Computer configuration and simulation software	CPU		Intel (R) 3.32 GHz
	RAM		128 GB
	Software		MATLAB, Ansys HFSS
	Simulation methods		FEBI, MLFMM
The structural parameters of the lens	F	Focal length (mm)	100
	D	Diameter lens (mm)	100
	ε_r	Relative permittivity	5.34
	μ_r	Relative permeability	1
	ε_{ML}	Relative permittivity of matching layer	$\sqrt{5.34}$
	$\tan\delta$	Dielectric loss tangent	0.0081
	f	Frequency (GHz)	28

Using the advanced electromagnetic field calculation software Ansys HFSS, the authors model the structures and compute the radiation characteristics of the modified-PPE lens antenna. This design incorporates a matching reflection layer applied to both the inner and outer surfaces of the lens and evaluated across four different lens types. The simulation results and detailed analyses are presented as follows.

A. Simulation Results

1) Radiation pattern

Fig. 9 illustrates the differences in the radiation patterns of lens antennas with different structural configurations. Three scenarios are considered: (1) two Matching Layers (MLs) applied to both the inner and outer surfaces of the lens, (2) a single ML applied to the inner surface, and (3) no ML applied. The results clearly show that lens antennas with MLs exhibit superior radiation patterns compared to those without MLs.

Specifically, in the case without an ML, the lens antenna with the Abbe sine condition structure achieves a maximum gain of 26.18 dBi. Meanwhile, the maximum gain values for lens antennas with plano-convex, hyperbolic shape, and straight-line condition structures are 26.00 dBi, 25.95 dBi, and 25.57 dBi, respectively. In contrast, when an ML is applied to the inner surface of the lens, the maximum gain of all lens antenna configurations is significantly improved. Notably, the maximum gain of the lens antenna with the straight-line condition structure increases the most, by 1.42 dB, from 25.57 dBi to 26.99 dBi. Furthermore, when two MLs are applied to both the inner and outer surfaces of the lens, the maximum gain of the lens antennas increases further. This highlights the crucial role of matching layers in enhancing the radiation efficiency of dielectric lens antennas. The maximum gain values of PPE lens antennas with Abbe sine condition, plano-convex, straight-line condition, and hyperbolic structures are 27.83 dBi, 27.82 dBi, 27.74 dBi, and 27.73 dBi, respectively.

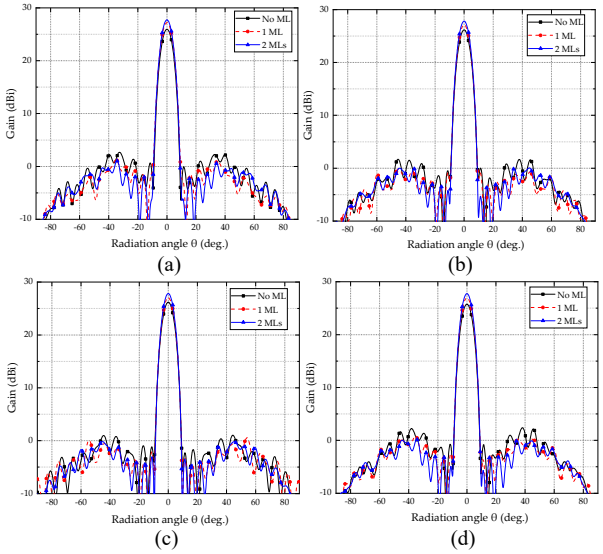

Fig. 9. Straight-line condition lens; Radiation patterns of PPE lens antennas with and without matching layers; (a). Hyperbol lens, (b). Plano-convex lens, (c). Abbe sine condition lens, (d). Straight-line condition lens.

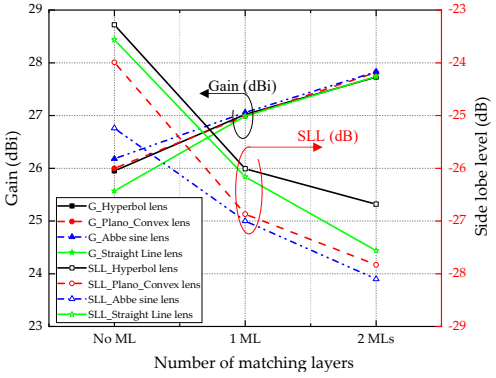

Fig. 10. Variation in maximum gain and side-lobe level.

The variation in the maximum gain and side-lobe level with and without the ML for different lens configurations is shown in Fig. 10. From the graph, it can be observed that

applying the ML to the lens reduces the side-lobe level in all cases. The most significant reduction occurs in the lens antenna with the straight-line condition, decreasing by 4 dB, from −23.56 dB to −27.56 dB. This is followed by the plano-convex, hyperbolic, and Abbe sine structures, which exhibit reductions of 3.84 dB, 3.4 dB, and 2.86 dB, respectively. However, the side-lobe level of the lens antenna with the Abbe sine condition consistently remains lower than −28.10 dB.

2) The electromagnetic field distributions on the xOz plane

Fig. 11 illustrates the electromagnetic field distribution of the lens antenna with four different lens structures. Two scenarios are considered: (1) without a Matching Layer (ML) and (2) with two MLs applied to both the inner and outer surfaces of the lens, on the xOz plane. The diagram shows that, without an ML, the electromagnetic field distribution between the lens and the radiation source is rough. In some cases, the field is completely canceled out before reaching the lens. The spherical wave from the radiation source and the planar wave behind the lens become indistinct due to partial energy reflection, which causes wave interference. In contrast, when two MLs are applied, the field distribution becomes smoother and more uniform. The planar wave behind the lens is also more clearly visible. These results demonstrate the effectiveness of MLs in enhancing the radiation characteristics of the lens antenna.

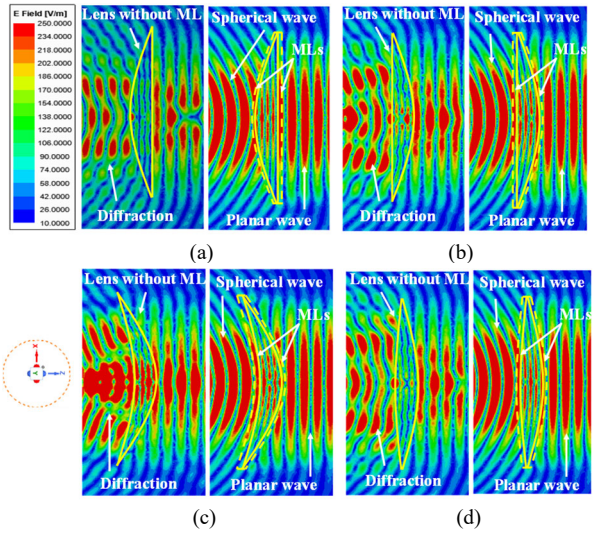

Fig. 11. The electromagnetic field distributions of lens antennas with and without MLs; (a). Hyperbol lens, (b). Plano-convex lens, (c). Abbe sine condition lens, (d). Straight-line condition lens.

B. The multi-beam PPE lens antenna with MLs

1) The multi-beam lens antenna structure

In this section, a lens antenna with Matching Layers (MLs) applied to both the inner and outer surfaces is proposed. Multiple feed horns are used to evaluate the antenna's ability to generate multi-beam. Fig. 12 illustrates the structure of the multi-beam lens antenna. The feed horns are arranged along a circular arc with a diameter equal to the lens's focal length ($R = F$). Each feed horn directs its emission toward the lens at an incident angle of α. The incident angles are set to $\alpha = 0°$, $\alpha = 15°$, $\alpha = 30°$, and $\alpha = 45°$, with a step size of 15°.

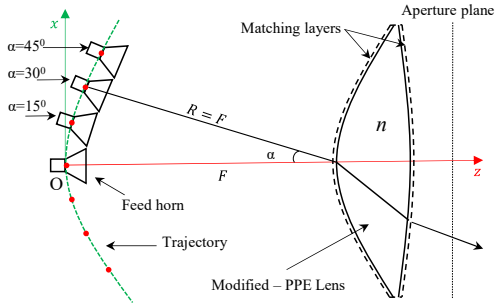

Fig. 12. The multi-beam lens antenna structure.

Four lens antenna structure models, including hyperbolic, Abbe sine condition, plano-convex, and straight-line condition, with two MLs applied, have been modeled and simulated using the electromagnetic field calculation software Ansys HFSS, with the feed horns placed along the trajectory $R = F$. The simulation results are analyzed, evaluated, and presented as follows:

2) Simulation results

a) The radiation patterns of the multi-beam lens antennas

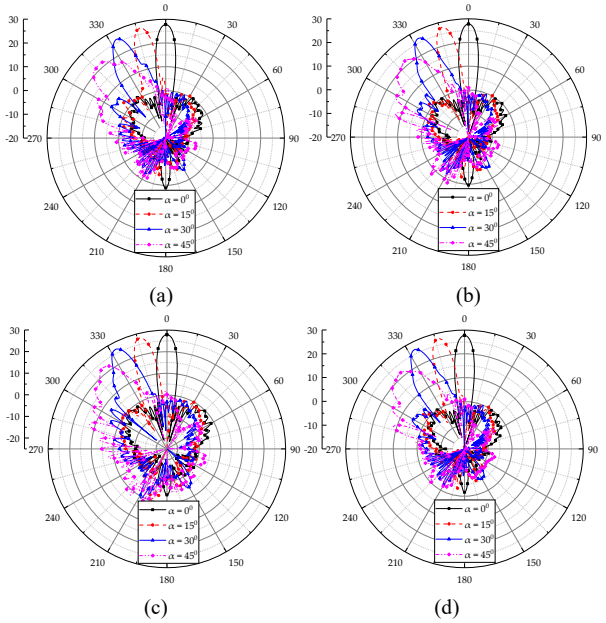

Fig. 13. The radiation pattern of the multi-beam PPE lens antenna; (a). Hyperbol lens, (b). Plano-convex lens, (c). Abbe sine condition lens, (d). Straight-line condition lens.

The radiation pattern of the four PPE lens antenna types, with radiation angles ranging from 0° to 45°, is shown in Fig. 13. When the feed horns are positioned along the same trajectory (R = F) with varying incident angles, the Abbe sine condition lens consistently achieves the highest maximum gain among the four structures. However, this gain decreases as the incident angle (α) increases. When the feed horn is placed at the focal point of the lens (α = 0°), the Abbe sine condition lens antenna reaches a maximum gain of 27.83 dBi. In comparison, the straight-line, plano-convex, and hyperbolic lens antennas achieve gains of 27.74 dBi, 27.82 dBi, and 27.73 dBi, respectively. At an incident angle of 45°, the Abbe sine condition lens

maintains a maximum gain of 22.77 dBi, which is 1.06 dB higher than the hyperbolic lens. The plano-convex and straight-line lens antennas achieve maximum gains of 21.96 dBi and 21.88 dBi, respectively.

b) A comparison graph of gain and SLL for the 4 types of lenses

The variation in side-lobe level and maximum gain is shown in Fig. 14. As the incident angle (α) increases, the side-lobe level of the lens antenna rises. This change becomes more noticeable when the feed horn is set at α = 30° and α = 45°. Among the different lens structures, the Abbe sine condition lens maintains the lowest side-lobe level at −9.43 dB. Additionally, this study evaluates the multi-beam capability of lens antennas with different structural configurations. The evaluation is based on parameters such as Half-Power Beamwidth (HPBW) and the deviation angle (θ_s) of the wave exiting the lens aperture relative to the radiation axis (Oz). Detailed results are presented in Table II.

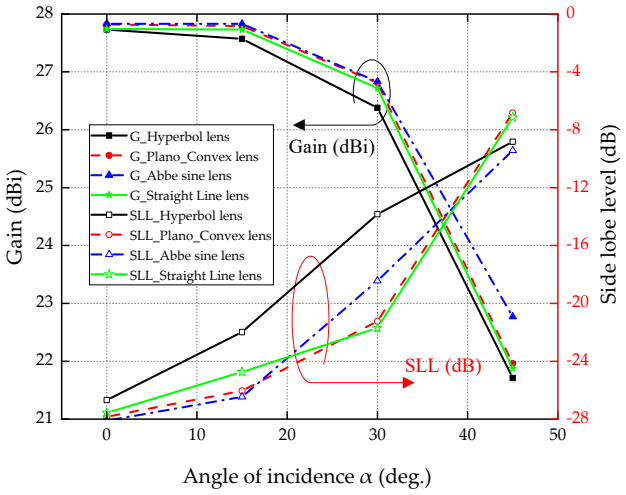

Fig. 14. The change in the radiation characteristics of the lens antenna as α varies.

c) Comparison ruselts

Table III compares the results of this study with previous research on lens antennas for multi-beam generation at the 28 GHz band. The comparison focuses on incidence angles of α = 0° and α = 30°. The table shows that lens antenna structures (Abbe Sine, Straight-line, Hyperbolic) with two Matching Layers (MLs) achieve higher gain when the feed horns are placed at the focal point (α = 0°) or at an off-focus position (α = 30^0). Additionally, these structures exhibit a lower side-lobe level than those reported in studies [20, 25−27, 37, 38]. These findings highlight the effectiveness of the proposed lens antenna design.

V. Conclusion

Using MATLAB software and Ansys HFSS electromagnetic field simulation software, the authors have performed the calculation, design, and simulation of four lens antenna structures with hyperbolic, plano-convex, Abbe sine, and straight-line conditions; each applied with matching layers. Through the analysis and evaluation of the simulation results, it can be observed that the proposed lens antenna structures, with matching layers applied to both the inner and outer surfaces of the lens, exhibit higher gain values compared to those of lens antenna structures without matching layers. The maximum gain of the straight-line condition lens antenna increased by 2.17 dB, while the maximum gains of the plano-convex, hyperbolic, and Abbe sine lens antennas were 1.82 dB, 1.78 dB, and 1.65 dB, respectively. In addition, in this paper, the authors place multiple feed horns along a defined trajectory. The results show that the lens antenna with matching layers is capable of generating multiple beams, with a maximum gain of 22.77 dBi at an incident angle of 45°. The results of this paper provide a foundation for researchers, manufacturers, and developers to apply appropriate lens antenna structures for base station antenna systems in next-generation mobile communications.

TABLE II. Simulation Results

		Hyperbolic lens				**Plano-convex lens**				**Abbe sine condition lens**				**Straight-line condition lens**			
	α (deg.)	Gain (dBi)	SLL (dB)	HPBW (deg.)	θ_s (deg.)	Gain (dBi)	SLL (dB)	HPBW (deg.)	θ_s (deg.)	Gain (dBi)	SLL (dB)	HPBW (deg.)	θ_s (deg.)	Gain (dBi)	SLL (dB)	HPBW (deg.)	θ_s (deg.)
Without ML	0	25.95	−23.28	7.3	0	26	−23.99	7.29	0	26.18	−25.24	7.35	0	25.57	−23.56	7.34	0
	15	25.66	−20.34	7.43	13.3	25.98	−23.66	7.39	13.7	26.21	−22.62	7.34	14	25.81	−22.79	7.38	13.6
	30	25.06	−13.95	8.03	26.5	25.46	−18.67	7.92	27.3	25.62	−18.16	7.95	27.8	25.42	−16.27	7.94	27
	45	21.54	−5.69	14.77	40.1	22.85	−3.75	12.55	40.3	23.05	−4.7	11.06	39.9	21.84	−3.27	11.99	40.4
1 ML	0	27.02	−26.01	7.19	0	26.99	−26.87	7.17	0	27.06	−27	7.2	0	26.99	−26.16	7.16	0
	15	26.72	−22.18	7.29	13.3	26.94	−25.00	7.21	13.7	27.05	−21.11	7.21	14.00	26.92	−24.58	7.28	13.7
	30	25.83	−14.33	8	26.7	26.21	−20.37	8.08	27.4	26.25	−18.34	7.92	27.8	26.19	−21.13	7.92	27.2
	45	21.76	−5.39	15.31	40.7	21.87	−2.51	18.42	40.1	22.07	−5.29	9.92	39.9	21.82	−1.85	17.65	40.5
2 MLs	0	27.73	−26.68	7.1	0	27.82	−27.83	7.08	0	27.83	−28.1	7.07	0	27.74	−27.56	7.06	0
	15	27.57	−21.98	7.12	13.3	27.79	−26.04	7.13	13.6	27.83	−26.46	7.11	13.9	27.73	−24.74	7.15	13.5
	30	26.38	−13.84	8.1	26.5	26.81	−21.23	7.93	27.1	26.83	−18.44	7.96	27.4	26.72	−21.7	7.97	26.9
	45	21.71	−4.76	15.16	41.3	21.96	−2.05	18.41	39.9	22.77	−4.65	11.13	38.3	21.88	−7.14	18.07	21.88

TABLE III. COMPARISON RESULTS

Ref.	Freq. (GHz)	α (deg.)	Abbe sine lens		Straight-line lens		Hyperbolic lens		Coplanar cylindrical lens		Rotma lens		Planar lens	
			Gain (dBi)	SLL (dB)	Gain (dBi)	SLL (dB)	Gain (dBi)	SLL (dB)	Gain (dBi)	SLL (dB)	Gain (dBi)	SLL (dB)	Gain (dBi)	SLL (dB)
[20]	28	0°	27.25	−23.18	27.48	−25.10	26.93	−21.68						
		30°	25.14	−20.5	25.5	−20.54	25.11	−18.67						
[25]	28	0°							21.24	−18.59				
		30°							20.99	−8.33				
[26]	28.5	0°									18.5			
		30°									17.00			
[27]	26	0°											22.2	−14.77
		25°											20.06	−8.00
[37]	28	0°	27.77		27.69									
		30°	26.92		26.41									
[38]	28	0°	27.48											
		30°	25.54	−11.65										
This work	28	0°	**27.83**	**−28.10**	**27.74**	**−27.56**	**27.73**	**−26.68**						
		30°	**26.83**	**−18.44**	**26.72**	**−21.7**	**26.38**	**−13.84**						

CONFLICT OF INTEREST

The authors declare no conflict of interest.

AUTHOR CONTRIBUTIONS

Nguyen Thi Dieu Linh developed the theoretical framework and supervised the project. Phan Van Hung conducted the simulations and data analysis. Nguyen Quoc Dinh and Tong Van Luyen reviewed and wrote the manuscript; All authors approved the final version.

FUNDING

This research is supported by Hanoi University of Industry [Grant number: 26-2023-RD/HĐ-ĐHCN].

REFERENCES

[1] W. Hong *et al.*, "Multibeam antenna technologies for 5G wireless communications," *IEEE Transactions on Antennas and Propagation,* vol. 65, no. 12, pp. 6231–6249, Dec 2017.

[2] L. Guangyi and J. Dajie, "5G: vision and requirements for mobile communication system towards year 2020," *Chinese Journal of Engineering,* vol. 2016, pp. 1−8, Apr 2016.

[3] S. Kumar *et al.,* "Fifth generation antennas: a comprehensive review of design and performance enhancement techniques," *IEEE Access.* 2020, p. 1, Sep 2020.

[4] Z. Sipus and T. Komljenovic, "Multi-Shell radially symmetrical lens antennas," *Aperture Antennas for Millimeter and Sub-Millimeter Wave Applications*, pp. 37–73, 2018.

[5] S. Sun, T. Rappaport, R. Heath, A. Nix, and S. Rangan, "MIMO for millimeter-wave wireless communications: beamforming, spatial multiplexing, or both?" *IEEE Communications Magazine*, vol. 52, no. 12, pp. 110–121, 2014.

[6] N. Vukmirovic *et al.,* "Position estimation with a millimeter-wave massive MIMO system based on distributed steerable phased antenna arrays," *EURASIP Journal on Advances in Signal Processing*, vol. 2018, pp. 1–17, Jun 2018.

[7] J. Zhang *et al.,* "Prospective multiple antenna technologies for beyond 5G," *IEEE Journal on Selected Areas in Communications*, vol. 38, pp. 1637–1660, 2019.

[8] A. N. Plastikov and B. L. Kogan, "Bifocal reflector antenna design procedure for wide-angle multi-beam applications," in *Proc. European Conference on Antennas and Propagation (EuCAP)*, Gothenburg, Sweden, Apr 2013.

[9] K. Ueno, "Multibeam antenna using a phased array fed reflector," *in Proc. IEEE Antennas and Propagation Society International Symposium,* Florida, USA, Aug. 1997, pp. 840–843.

[10] Y. Chen, H. Meng, Y. Gan, and W. Dou, "Millimeter wave multi-beam reflector antenna," in *Proc. 2018 International Workshop on Antenna Technology (iWAT)*, Nanjing, China, 2018, pp. 1–3.

[11] F. Fan, M. Cai, J. Zhang, Z. Yan, and J. Wu, "Wideband lowprofile luneburg lens based on a glide-symmetric metasurface," *IEEE Access*, vol. 8, pp. 85698–85705, 2020.

[12] K. L. Chung, S. Chaimool, and C. Zhang, "Wideband subwavelength-profile circularly polarised array antenna using anisotropic metasurface," *Electronics Letters*, vol. 51, no. 18, pp. 1403–1405, 2015.

[13] G. A. Egorov and G. V. Eleftheriades, "Theory and simulation of metasurface lenses for extending the angular scan range of phased arrays," *IEEE Transactions on Antennas and Propagation*, vol. 68, no. 5, pp. 3705–3717, 2020.

[14] K. L. Chung, X. Yan, S. Chaimool, B. Feng, and Y. Li, "On the surface susceptibilities and effective parameters of metasurfaces composed of isolated metallic unit-cells," *International Journal of RF and Microwave Computer-Aided Engineering*, pp. 1–9, 2020.

[15] C. Xue, Q. Lou, and Z. N. Chen, "Broadband double-layered huygens' metasurface lens antenna for 5G millimeter-wave systems," *IEEE Transactions on Antennas and Propagation*, vol. 68, no. 3, pp. 1468–1476, 2020.

[16] O. Yesilyurt and G. Turhan-Sayan, "Metasurface lens for ultra-wideband planar antenna," *IEEE Transactions on Antennas and Propagation*, vol. 68, no. 2, pp. 719–726, 2020.

[17] Y. H. Lv, X. Ding, B.-Z. Wang, and D. E. Anagnostou, "Scanning range expansion of planar phased arrays using metasurfaces," *IEEE Transactions on Antennas and Propagation*, vol. 68, no. 3, pp. 1402–1410, 2020.

[18] N. Q. Dinh, N. T. Binh, Y. Yamada, and N. Michishita, "Proof of the density tapering concept of an unequally spaced array by electric field distributions of electromagnetic simulations," *Journal of Electromagnetic Waves and Applications*, vol. 34, no. 5, pp. 668–681, 2020.

[19] Y Tajima and Y Yamada, "Design of shaped dielectric lens antenna for wide angle beam steering," *Electron Commun Jpn.* vol. 89, pp. 286–296, 2006.

[20] P. V. Hung, N. Q. Dinh, and Y. Yamada, "Negative refractive index-shaped lens antenna with straight line condition for wide angle beam scanning," *Journal of Electromagnetic Waves and Applications*, vol. 36, no. 6, pp. 856–874, 2021.

[21] H. Giddens and Y. Hao, "Multibeam graded dielectric lens antenna from multimaterial 3-D printing," *IEEE Trans. Antennas Propag.,* vol. 68, no. 9, pp. 6832–6837, 2020.
[22] T. Maruyama, K. Yamamori, and Y. Kuwahara, "Design of multibeam dielectric lens antennas by multiobjective optimization," *IEEE Trans. Antennas Propag.*, vol. 57, no. 1, pp. 57–63, 2009.
[23] Y. Tajima and Y. Yamada, "Simulation of a shaped dielectric lens antenna by FEKO," *Appl. Comput. Electromagn. Soc. J.,* vol. 24, no. 4, pp. 419–426, 2009.
[24] P. V. Hung *et al.,* "Estimations of matching layers effects on lens antenna characteristics," in *Proc. EAI INISCOM 2020 - 6th EAI International Conference on Industrial Networks and Intelligent System*, pp. 85–94, 2020.
[25] Y. S. Zhang and W. Hong, "A millimeter-wave gain enhanced multi-beam antenna based on a coplanar cylindrical dielectric lens," *IEEE Transactions on Antennas and Propagation*, vol. 60, no. 7, pp. 3485–3488, 2012.
[26] E. G. Marin, D. Filipovic, J. M. Campos, and P. S. Olivares, "Low-cost lens antenna for 5G multi-beam communication," *Microwave and Optical Technology Letters*, vol. 62, 2020.
[27] Y. J. Cheng, W. Hong, K. Wu, Z. Q. Kuai, C. Yu, J. X. Chen, J. Y. Zhou, and H. J. Tang, "Substrate Integrated Waveguide (SIW) rotman lens and its Ka-band multibeam array antenna applications," *IEEE Transactions on Antennas and Propagation*, vol. 56, no. 8, pp. 2504–2513, 2008.
[28] M. J. M. V, D. Vorst *et al.,* "Effect of internal reflections on the radiation properties and input impedance of integrated lens antennas-comparison between theory and measurements," *IEEE Transactions on Microwave Theory and Techniques*, vol. 49, no. 6, pp. 1118−1125, June 2001.
[29] G. Godi, R. Sauleau, and D. Thouroude, "Performance of reduced size substrate lens antennas for millimeter-wave communications," *IEEE Trans. Antennas Propag.*, vol. 53, pp. 1278–1286, 2005.
[30] A. Neto, S. Maci, P. J. I. D. Maagt, "Reflections inside an elliptical dielectric lens antenna," *IEEE Proc. Microw. Antennas Propag*, vol. 145, no. 3, pp. 243–247, 1998.
[31] N. T. Nguyen, R. Sauleau, and P. Martinez, "Very broadband extended hemispherical lenses: Role of matching layers for bandwidth enlargement," *IEEE Trans. Antennas Propag,* vol. 57, pp. 1907–1913, 2009.
[32] F Tokan, "Matching layer design procedure for a novel broadband dielectric lens antenna," pp. 149–198, 2013.
[33] J. A. Stratton, *Electromagnetic Theory*, McGraw-Hill Book Company, Inc., New York, 1994.
[34] Y. Tajima and Y. Yamada, "Design of shaped dielectric lens antenna for wide angle beam steering," *Electronics and Communications in Japan (Part III: Fundamental Electronic Science)*, vol. 89, pp. 1–12, Feb 2006.
[35] S. Lee and Y. Lo, *Antenna Handbook: Theory, Applications, and Design*, Van Nostrand Reinhold, 1988.
[36] A. W. Rudge and K. Milne, *The Handbook of Antenna Design*, Rudge, vol. 2, Iet, 1982.
[37] F. Ansarudin, T. A. Rahman, Y. Yamada, N. Rahman, and K. Kamardin, "Multi beam dielectric lens antenna for 5G base station," *Sensors*, vol. 20, no. 5849, pp. 1−17, 2020.
[38] S. Hamid, N. Rahman, Y. Yamada, P. Hung, and Q. D. Nguyen, "Multibeam characteristics of a negative refractive index shaped lens," *Sensors*, vol. 20, no. 5703, pp. 1−17, 2020.